Theoretical realization of three-dimensional nanolattice structure fabrication based on high-order waveguide-mode interference and sample rotation

Xiangxian Wang[1] · Huan Tong[1] · Zhiyuan Pang[1] · Jiankai Zhu[1] · Xiaoxiong Wu[1] · Hua Yang[1] · Yunping Qi[2]

Abstract

A theoretical method of using high-order waveguide-mode interference combined with sample rotation is proposed to fabricate different kinds of three-dimensional nanolattice structures. The lithography sample is assisted by an asymmetric metal-cladding dielectric waveguide structure. High-order waveguide modes can be excited in the photoresist layer by both transverse magnetic and transverse electric polarized light. By utilizing multiple exposures of high-order waveguide-mode interference combined with sample-rotation, various three-dimensional nanolattice structures can be obtained. The resulting optical field distributions are simulated using the finite element method in this study, and sample rotation is expressed by coordinate matrix transformation. As examples, the three-dimensional optical field distributions resulting from fifth-order waveguide-mode interference were simulated with 90° and 60° sample rotations and multiple exposures. The results show that a quasi-cuboid structure with a simple tetragonal arrangement and a quasi-hexagonal structure with a hexagonal close-packed lattice can be obtained. Moreover, the numerical simulation results revealed that the shapes, sizes, arrangements, and periods of the structures can be controlled by the rotation method, photoresist thickness, waveguide modes used for exposure, and so on.

✉ Xiangxian Wang
wangxx869@126.com

1 School of Science, Lanzhou University of Technology, Lanzhou 730050, China

2 College of Physics and Electronic Engineering, Northwest Normal University, Lanzhou 730070, China

1 Introduction

In recent years, the application of nanostructures has become increasingly diverse in materials, physics, and chemistry (Zheng and Yang 2018; Liang et al. 2019; Zhao et al. 2018a, b; Cen et al. 2018a, b; Lv et al. 2018), including applications in photocatalysis (Ye et al. 2018; Yan et al. 2018), surface-enhanced Raman scattering (Liu et al. 2015a, b; Yu et al. 2018), absorption enhancement (Cen et al. 2018a, b), metamaterials (Liu et al. 2015a, b; Chen et al. 2016a, b; Shao et al. 2017), sensors (Wei et al. 2017; Wang et al. 2018; Liu et al. 2018; Chen et al. 2016a, b), Fano resonances (Yang et al. 2017; Zhao et al. 2018a, b), high-performance batteries (Su et al. 2018), terahertz plasma wave (Li et al. 2018; Du et al. 2018), optical tweezers (Mohammadnezhad and Hassanzadeh 2017a, b), and so on. Thus, nanostructure fabrication is an important process. Various nanostructure fabrication methods have consequently been proposed, such as laser interference lithography (Hassanzadeh et al. 2015), electron beam lithography (Utke et al. 2008; Gunnarsson et al. 2005), atomic-force microscopy (Chien et al. 1999), ultraviolet (UV) lithography (Bogaerts et al. 2002), extreme UV lithography (Gwyn et al. 1998), X-ray lithography (Feiertag et al. 1997), and surface plasmon interference lithography (Murukeshan and Sreekanth 2015; Wang et al. 2019). Compared with these methods, waveguide-mode (WM) interference lithography has the advantages of short exposure time and low heat loss. Wang et al. (2011) experimentally and theoretically demonstrated a sub-wavelength lithography method in which two metallic nano-slits are used to excite transverse electric (TE) mode interference. In our early work, we successfully demonstrated large-area maskless sub-wavelength lithography by employing WM interference (Wang et al. 2013). To fabricate sub-wavelength gratings with different periods, we further proposed a method involving a zeroth-order WM interference nanolithography configuration based on an asymmetric metal-cladding dielectric waveguide structure and studied the factor that could influence the period (Wang et al. 2016, 2017a, b). We subsequently employed an asymmetric metal-cladding dielectric waveguide structure to excite two interfering high-order WMs to fabricate hierarchical sub-wavelength structures (Wang et al. 2017a, b). However, these methods are suitable only for one- or two-dimensional (2D) structures. Recently, we successfully fabricated 2D surface relief gratings by rotating the sample by 90° (Wang et al. 2015). Hassanzadeh et al. (2015) changed the number of exposures with a corresponding rotation method and thereby generated various sophisticated geometries. These experimental and simulated results demonstrated that laser interference lithography combined with sample rotation can realize the fabrication of a variety of low-cost periodic nanoscale patterns over a large area. In addition, we previously proposed a theoretical method to fabricate micro-optical structures involving sample rotation with multiple and continuous exposures (Chen et al. 2017). Furthermore, we proposed a new nanolithography technique for 2D subwavelength structures by employing sample rotation with zeroth-order waveguide mode interference (Pang et al. 2018). However, although the structures were fabricated by laser interference lithography with sample rotation (Hassanzadeh et al. 2015; Chen et al. 2017), the periods of the structures were larger than half of the wavelength; thus, these fabrication methods cannot be employed beyond the diffraction limit. To overcome the dimensional and diffraction limits, we propose a theoretical method of fabricating three-dimensional (3D) nanolattice structures by rotating the sample and performing multiple exposures. Analysis of the simulated optical field intensity distributions revealed that the shapes and sizes of the nanostructures can be controlled by the rotation method, photoresist thickness, WMs used for exposure, and so on. Thus, a series of complex structures could be obtained.

2 Theoretical analysis

Figure 1 presents a schematic of high-order WM interference lithography combined with sample rotation, which is similar to the method that we previously used to generate WM interference by transverse magnetic (TM) or TE WMs (Wang et al. 2017a, b), except that this method includes sample rotation. The XY plane corresponds to the interface between the Ag film and photoresist, and the positive Z axis is directed toward the Ag film layer. By using this configuration and rotating the sample $N - 1$ times with N exposures, 3D nanolattice structures can be obtained. The resulting optical field distributions were numerically simulated in this study by using the finite element method (Zhang et al. 2018; Qi et al. 2018). A 442 nm laser was used as the excitation light, and a 45-nm-thick Ag film with a dielectric constant of $-0.57018 + 0.7514i$ was employed as the metal layer. The refractive indices of the prism and photoresist were 1.6 and 1.7, respectively, and the photoresist thickness was set to 950 nm. In this case, the excitation angles for TE_5 and TM_5 WMs were 44.73° and 50°, respectively.

To analyze the rotation and exposure process, the matrix representation of a coordinate transformation can be used, as we described in our previous work (Chen et al. 2017). The coordinate matrix transformation can be expressed as

$$\left(X_n, Y_n, Z_n\right) = (X, Y, Z) \begin{pmatrix} \cos\alpha_n & \sin\alpha_n & 0 \\ -\sin\alpha_n & \cos\alpha_n & 0 \\ 0 & 0 & 1 \end{pmatrix}, \tag{1}$$

where (X, Y, Z) is the initial spatial position of the sample, and α_n is the rotation angle. The optical field distributions $I(X, Y, Z)$ can be calculated by using the finite element method. After the first exposure, the sample was rotated by a certain angle, followed by a second exposure for the same time. The optical field intensity remained unchanged, while the exposed spatial position of the sample changed and could be expressed by using Eq. (1), so the optical field spatial distributions $In(Xn, Yn, Zn)$ could be calculated. The final optical field distributions of high-order WM interference with multiple exposures could be obtained by summing the distributions corresponding to each exposure. Note that the optical field of the WM in the photoresist layer is a standing wave field, and the node number of the standing wave corresponds to the mode order number of WM, which we can use to fabricate a 3D nanostructure. Since our high-order WM interference lithography configuration is based on a prism coupling technique, the optical intensity can be effectively

Fig. 1 Schematic of high-order WM interference lithography combined with sample rotation (color online)
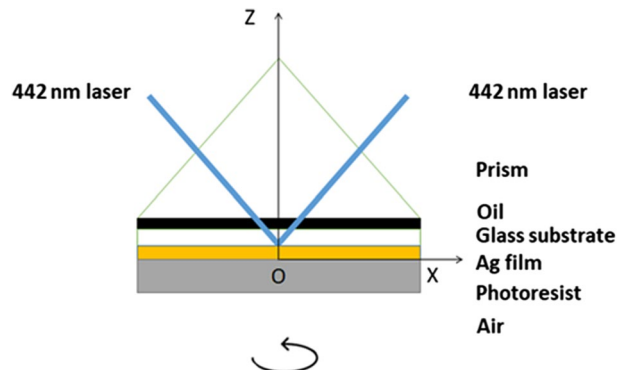
approximated without considering the influence of propagation loss in the photoresist layer. Thus, we assume the refractive index of the photoresist as a real number in the calculation (Murukeshan and Sreekanth 2015; Wang et al. 2013). By analyzing the 3D optical field distributions, the shapes, sizes, arrangements, and periods of nanolattice structures could be obtained.

## 3 Numerical simulation results

After performing the above analysis, we simulated the optical field distributions of TE_5 and TM_5 throughout the photoresist with no sample rotation. The results are depicted in Fig. 2a, b. The optical field distributions were simulated from -420 to 420 nm along both the X and Y axes. The periods of these hierarchical sub-wavelength structures for TE_5 and TM_5 are 200 nm and 180 nm, respectively, in the X direction.

Based on Fig. 2, by exposing a sample twice for the same time and rotating it 90° after the first exposure, a periodic 3D nanolattice structure consisting of a number of quasi-cuboids could be recorded in the photoresist layer and the lattice arranged in a square in a plane parallel to XY plane. As an example, the optical field distributions corresponding to TE_5 WM interference are plotted in Fig. 3a. Because of the 90° sample rotation, the optical field distribution in the XZ plane is the same as that in the YZ plane. To clearly show the quasi-cuboid structures and to analyze the periods in different directions, cross-sections of the simulated optical field at $Z=-50$ nm and $X=-420$ nm are provided in Fig. 3b, c, respectively. Furthermore, Fig. 3d presents the optical field intensity distribution corresponding to Fig. 3b along the X axis at $Z=-50$ and $Y=0$ nm. Evidently, the periods in the X and Y directions are both 200 nm. The optical intensity distribution along the Z axis with both X and Y equal to 0 nm is shown in Fig. 3e, exhibiting a period of 170 nm. Figure 3f is an enlarged view of a single quasi-cuboid from Fig. 3a, which shows its dimensions in all directions clearly. The width and length of this quasi-cuboid are both 100 nm, and the height is 85 nm.

Figure 4a presents the optical field distributions generated by performing three exposures for the same time with 60° rotations after the first and second exposures. The optical field distribution obtained from the cross-section at $Z=-50$ nm in Fig. 4a is
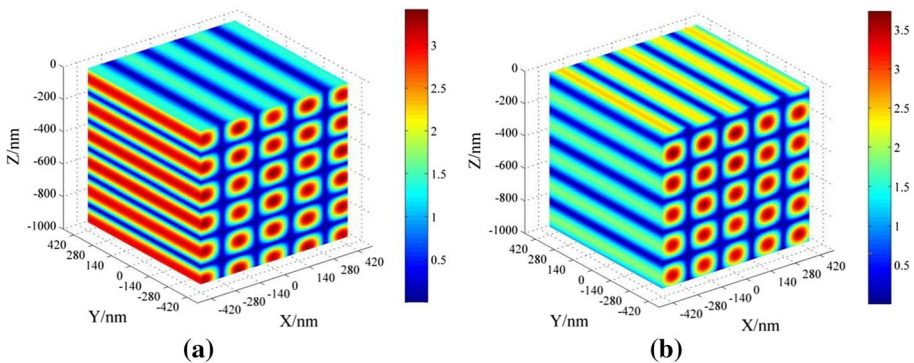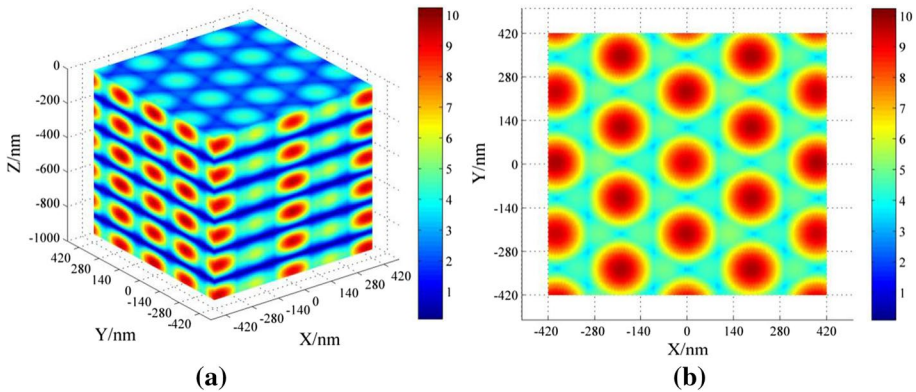

Fig. 2 Simulated 3D optical field distributions in the photoresist layer obtained by high-order WM interference from -420 to 420 nm along both the X and Y axes. **a** TE_5 interference. **b** TM_5 interference (color online)
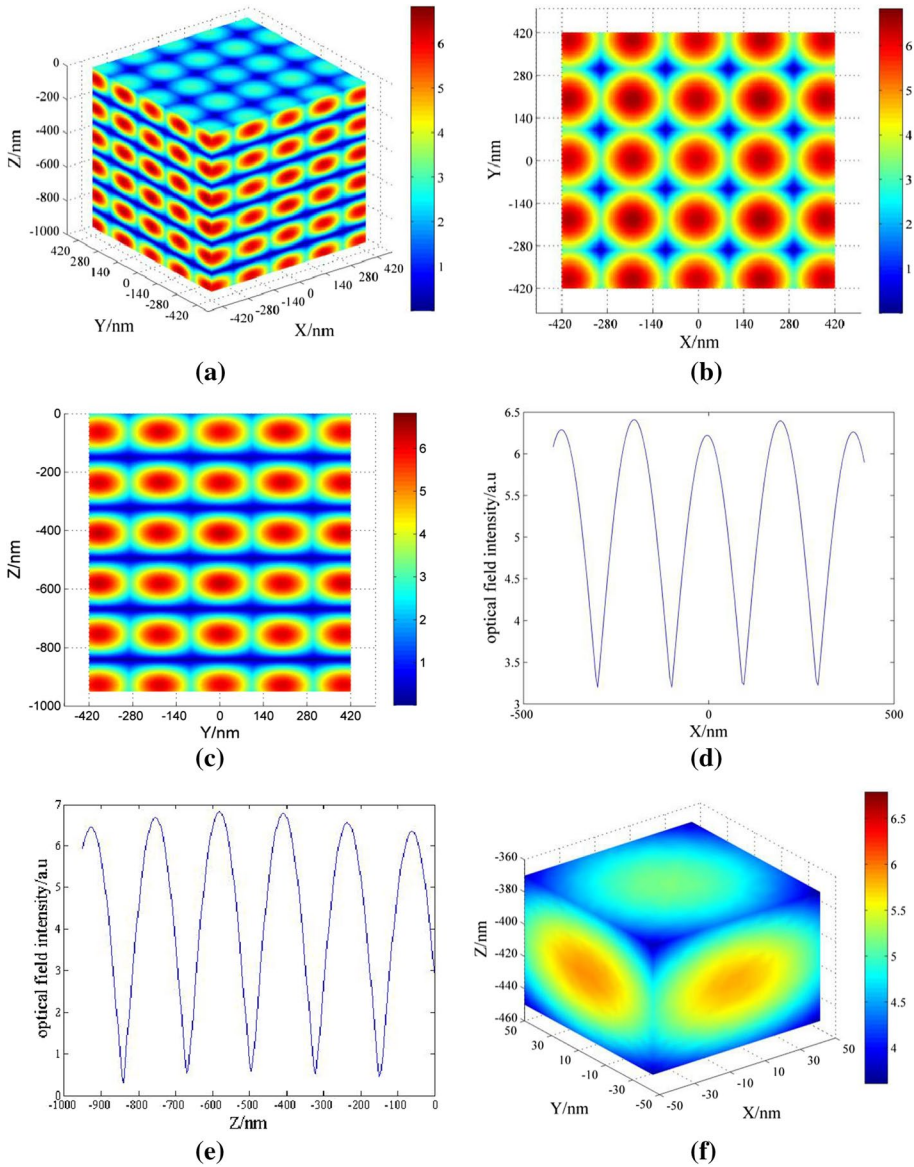
Fig. 3 a Simulated 3D optical field distributions of TE$_5$ WM interference obtained by exposing a sample twice for the same time with 90° rotation. **b** Optical field distribution of the cross-section of (**a**) at Z=−50 nm. **c** Optical field distribution of the cross-section at X=−420 nm in (**a**). **d** Optical intensity distribution in (**b**) along the X axis at Z=−50 and Y=0 nm. **e** Optical intensity distribution in (**c**) along the Z axis at X=0 and Y=0 nm. **f** Enlarged view of a single quasi-cuboid from (**a**) (color online)

shown in Fig. 4b. A 3D nanolattice structure with quasi-hexagonal dots regularly and periodically patterned in the photoresist layer is evident. This pattern reveals a hexagonal close-packed lattice structure parallel to the XY plane, which was obtained by using TE$_5$ WM interference. In this case, the period in the Z direction is 170 nm, which is the

Fig. 4 **a** Simulated 3D optical field distributions with TE_5 WM interference after three sample exposures for the same time with two 60° rotations. **b** Optical field distribution of the cross-section of (**a**) at $Z = -50$ nm (color online)

same as that in Fig. 3. Meanwhile, in the plane parallel to the XY plane, the separation between adjacent dots is 230 nm. Each dot is quasi-hexagonal, and seven dots form a hexagonal close-packed lattice structure, while three dots form an equilateral triangle. The heights of all of the equilateral triangles are the same, approximately 200 nm, which is the same as the period of the quasi-cuboids in Fig. 3.

4 Conclusion

In this paper, we proposed a method of fabricating 3D nanolattice structures by using high-order WM interference and sample rotation based on an asymmetric metal-cladding dielectric waveguide structure. Many WMs exist in the waveguide structure and can be adjusted according to the photoresist thickness and the polarization of the excitation laser. The shapes, sizes, arrangements, and periods of the fabricated structures can be changed by adjusting the sample rotation, photoresist thickness, and WMs used for exposure. As examples, we simulated the 3D optical field distributions resulting from using TE_5 WM interference and performing multiple exposures with sample rotation by 90° or 60°, and we found that a quasi-cuboid structure with a simple tetragonal arrangement and a quasi-hexagonal structure with a hexagonal close-packed lattice, respectively, could be fabricated. The method proposed in this work could potentially be used to fabricate a wide variety of 3D nanolattice structures and is expected to find numerous applications in the field of nano-optics. In this letter, we obtained a quasi-cuboid rather than a cube as the individual unit of arrangement. Future studies shall focus on the optical properties of the structures simulated in this study.

References

Bogaerts, W., Wiaux, V., Taillaert, D., Beckx, S., Luyssaert, B., Bienstman, P.: Fabrication of photonic crystals in silicon-on-insulator using 248-nm deep UV lithography. IEEE J. Sel. Top. Quantum Electron. **8**(4), 928–934 (2002)

Cen, C.L., Lin, H., Huang, J., Liang, C.P., Chen, X.F., Tang, Y.J., Yi, Z., Ye, X., Liu, J.W., Yi, Y.G., Xiao, S.Y.: A tunable plasmonic refractive index sensor with nanoring-strip graphene arrays. Sensors **18**, 4489 (2018a)

Cen, C.L., Chen, J.J., Liang, C.P., Huang, J., Chen, X.F., Tang, Y.J., Yi, Z., Xu, X.B., Yi, Y.G., Xiao, S.Y.: Plasmonic absorption characteristics based on dumbbell-shaped graphene metamaterial arrays. Physica E **103**, 93–98 (2018b)

Chen, J., Tang, C.J., Mao, P., Peng, C., Gao, D.P., Yu, Y., Wang, Q.G., Zhang, L.B.: Surface-plasmon-polaritons-assisted enhanced magnetic response at optical frequencies in metamaterials. IEEE Photon. J. **8**, 4800107 (2016a)

Chen, J., Zhang, T., Tang, C.J., Mao, P., Liu, Y.J., Yu, Y., Liu, Z.Q.: Optical magnetic field enhancement via coupling magnetic plasmons to optical cavity modes. IEEE Photon. Technol. Lett. **28**, 1529–1532 (2016b)

Chen, Y.Z., Wang, X.X., Wang, R., et al.: Theoretical study of micro-optical structure fabrication based on sample rotation and two-laser-beam interference. Chin. Phys. B **26**(5), 054203-1–054203-5 (2017)

Chien, F.S.S., Wu, C.L., Chou, Y.C., Chen, T.T., Gwol, S., Hsieh, W.F.: Nanomachining of (110)-oriented silicon by scanning probe lithography and anisotropic wet etching. Appl. Phys. Lett. **75**(16), 2429–2431 (1999)

Du, H.M., Zhang, L.P., Li, D.G.: THz plasma wave instability in field effect transistor with electron diffusion current density. Plasma Sci. Technol **20**, 115001 (2018)

Feiertag, G., Ehrfeld, W., Freimuth, H., Kolle, H., Lehr, H., Schmidt, M., Sigalas, M.M., Soukoulis, C.M., Kiriakidis, G., Pedersen, T., Kuhl, J., Koenig, W.: Fabrication of photonic crystals by deep x-ray lithography. Appl. Phys. Lett. **71**(11), 1441–1443 (1997)

Gunnarsson, L., Rindzevicius, T., Prikulis, J., Kasemo, B., Kall, M., Zou, S., Schatz, G.: Confined plasmons in nanofabricated single silver particle pairs: experimental observations of strong interparticle interactions. J. Phys. Chem. B **109**(3), 1079–1087 (2005)

Gwyn, C.W., Stulen, R., Sweeney, D., et al.: Extreme ultraviolet lithography. J. Vac. Sci. Technol., B **16**(6), 3142–3149 (1998)

Hassanzadeh, A., Mohammadnezhad, M., Mittler, S.: Multiexposure laser interference lithography. J. Nanophoton. **9**, 093067-1–093067-12 (2015)

Li, D.G., Zhang, L.P., Du, H.M.: The instability of terahertz plasma waves in cylindrical FET. Plasma Sci. Technol (2018). https://doi.org/10.1088/2058-6272/aaf874

Liang, C.P., Niu, G., Chen, X.F., Zhou, Z.G., Yi, Z., Ye, X., Duan, T., Yi, Y., Xiao, S.Y.: Tunable triple-band graphene refractive index sensor with good angle-polarization tolerance. Opt. Commun. **436**, 57–62 (2019)

Liu, G., Yu, M., Liu, Z., Liu, X., Huang, S., Pan, P., Wang, Y., Liu, M., Gu, G.: One-process fabrication of metal hierarchical nanostructures with rich nanogaps for highly-sensitive surface-enhanced Raman scattering. Nanotechnology **26**(18), 185702 (2015a)

Liu, Z.Q., Liu, X.S., Huang, S., Pan, P.P., Chen, J., Liu, G.Q., Gu, G.: Automatically acquired broadband plasmonic-metamaterial black absorber during the metallic film-formation. Appl. Mater. Interfaces **7**, 4962–4968 (2015b)

Liu, C., Su, W.Q., Liu, Q., Lu, X.L., Wang, F.M., Sun, T., Chu, P.K.: Symmetrical dual D-shape photonic crystal fibers for surface plasmon resonance sensing. Opt. Express **26**(7), 9039–9049 (2018)

Lv, J.W., Mu, H.W., Liu, Q., Zhang, X.M., Li, X.L., Liu, C., Jiang, S.S., Sun, T., Chu, P.K.: Multiwavelength unidirectional forward scattering in the visible range in all-dielectric silicon hollow nanodisk. Appl. Opt. **57**(17), 4771–4776 (2018)

Mohammadnezhad, M., Hassanzadeh, A.: Evanescent field interferometric optical tweezers with rotational symmetric patterns. J. Opt. Soc. Am. B **34**(5), 983–989 (2017a)

Mohammadnezhad, M., Hassanzadeh, A.: Multibeam interferometric optical tweezers. J Nanophoton. **11**(3), 036007 (2017b)

Murukeshan, V.M., Sreekanth, K.V.: Maskless plasmonic lithography for patterning of one- and two dimensional periodic features. Proc. SPIE **7637**, 76371G (2015)

Pang, Z.Y., Tong, H., Wu, X.X., Zhu, J.K., Wang, X.X., Yang, H., Ping, Q.Y.: Theoretical study of multiexposure zeroth-order waveguide mode interference lithography. Opt. Quant. Electron. **50**, 335 (2018)

Qi, Y.P., Zhang, X.W., Zhou, P.Y., Hu, B.B., Wang, X.X.: Refractive index sensor and filter of metal-insulator-metal waveguide based on ring resonator embedded by cross structure. Acta Phys. Sin. **67**(19), 197301 (2018)

Shao, H.Y., Chen, C., Wang, J.C., Pan, L., Sang, T.: Metalenses based on the non-parallel double-slit arrays. J. Phys. D Appl. Phys. **50**(38), 384001 (2017)

Su, W.X., Feng, W.J., Cao, Y., Chen, L.J., Li, M.M., Song, C.K.: Porous honeycomb-like carbon prepared by a facile sugar-blowing method for high-performance lithium–sulfur batteries. Int. J. Electrochem. Sci. **13**, 6005–6014 (2018)

Utke, I., Hoffmann, P., Melngailis, J.: Gas-assisted focused electron beam and ion beam processing and fabrication. J. Vac. Sci. Technol., B **26**(4), 1197–1276 (2008)

Wang, B., Chew, A.B., Teng, J.H., Si, G.Y., Danner, A.J.: Subwavelength lithography by waveguide mode interference. Appl. Phys. Lett. **99**(15), 151106 (2011)

Wang, X.X., Zhang, D.G., Chen, Y.K., Zhu, L.F., Yu, W.H., Wang, P., Yao, P.J., Ming, H., Wu, W.W., Zhang, Q.J.: Large area sub-wavelength azo-polymer gratings by waveguide modes interference lithography. Appl. Phys. Lett. **102**(3), 031103 (2013)

Wang, X.X., Wang, X.D., Yang, H., Ye, S., Yu, J.: Study of surface relief-gratings lithography of epoxy-based bisazobenzene polymer BP-2A-35-CN. J. Funct. Mater. **6**, 20132–20135 (2015)

Wang, R., Wang, X.X., Yang, H., Ye, S.: Theoretical investigation of adjustable period sub-wavelength grating inscribed by TE_0 waveguide modes interference lithography. Acta Phys. Sin. **65**(9), 094206 (2016)

Wang, R., Wang, X.X., Yang, H., Qi, Y.P.: Theoretical investigation of hierarchical sub-wavelength photonic structures fabricated using high-order waveguide-mode interference lithograph. Chin. Phys. B **26**(2), 024202 (2017a)

Wang, X.X., Wang, R., Yang, H., Qi, Y.P.: Inscription of sub-wavelength gratings with different periods based on asymmetric metal-cladding dielectric waveguide structure. Optik **140**, 261–267 (2017b)

Wang, X.X., Wu, X.X., Chen, Y.Z., Bai, X.L., Pang, Z.Y., Yang, H., Qi, Y.P., Wen, X.L.: Investigation of wide-range refractive index sensor based on asymmetric metal-cladding dielectric waveguide structure. AIP Adv. **8**, 105029 (2018)

Wang, X.X., Pang, Z.Y., Tong, H., Wu, X.X., Bai, X.L., Yang, H., Wen, X.L., Qi, Y.P.: Theoretical investigation of subwavelength structure fabrication based on multi-exposure surface plasmon interference lithography. Results Phys. **12**, 732–737 (2019)

Wei, Z.Q., Zhou, Z.K., Li, Q.Y., Xue, J.C., Falco, A.D., Yang, Z.J., Zhou, J.H., Wang, X.H.: Flexible nanowire cluster as a wearable colorimetric humidity sensor. Small **13**, 1700109 (2017)

Yan, Y.X., Yang, H., Zhao, X.X., Li, R.S., Wang, X.X.: Enhanced photocatalytic activity of surface disorder-engineered $CaTiO_3$. Mater. Res. Bull. **105**, 286–290 (2018)

Yang, L., Wang, J.C., Yang, L.Z., Hu, Z.D., Wu, X.J., Zheng, G.G.: Characteristics of multiple Fano resonances in waveguide-coupled surface plasmon resonance sensors based on waveguide theory. Sci. Rep. **8**, 2560 (2017)

Ye, Y.C., Yang, H., Zhang, H.M., Jiang, J.L.: A promising Ag_2CrO_4/$LaFeO_3$ heterojunction photocatalyst applied to photo-Fenton degradation of RhB. Environ. Technol. (2018). https://doi.org/10.1080/09593330.2018.1538261

Yu, M., Huang, Z., Liu, Z., Chen, J., Liu, Y., Tang, L., Liu, G.: Annealed gold nanoshells with highly-dense hotspots for large-area efficient Raman scattering substrates. Sens. Actuator B-Chem. **262**, 845–851 (2018)

Zhang, X.W., Qi, Y.P., Zhou, P.Y., Gong, H.H., Hu, B.B., Yan, C.M.: Refractive index sensor based on fano resonances in plasmonic waveguide with dual side-coupled ring resonators. Photon. Sens. **8**(4), 367–374 (2018)

Zhao, Q., Yang, Z.J., He, J.: Fano resonances in heterogeneous dimers of silicon and gold nanospheres. Front. Phys. **13**(3), 13780 (2018a)

Zhao, X.X., Yang, H., Li, S.H., Cui, Z.M., Zhang, C.R.: Synthesis and theoretical study of large-sized $Bi_4Ti_3O_{12}$ square nanosheets with high photocatalytic activity. Mater. Res. Bull. **107**, 180–188 (2018b)

Zheng, C.X., Yang, H.: Assembly of Ag_3PO_4 nanoparticles on rose flower-like Bi_2WO_6 hierarchical architectures for achieving high photocatalytic performance. J. Mater. Sci.: Mater. Electron. **29**(11), 9291–9300 (2018)